Recent developments of surface light scattering as a tool for optical-rheology of polymer monolayers

Pietro Cicuta [a,*], Ian Hopkinson [b]

[a] *Cavendish Laboratory, University of Cambridge, Madingley Road, Cambridge CB3 0HE, UK*
[b] *Department of Physics, U.M.I.S.T., Manchester M60 1QD, UK*

Abstract

Surface quasi-elastic light scattering (SQELS) is an application of dynamic light scattering to measure the dynamics of the thermal roughness of liquid surfaces. An analysis of the spectrum of thermal fluctuations provides information on surface properties like tension and elasticity. In this work we will focus particularly on its use to study polymer or polymer-like Langmuir monolayers. We review work in this area and give an up-to-date overview of the method. Important advances have very recently taken place in the theoretical understanding of this problem, and this has allowed improvements in the analysis of the experimental data. A practical method to estimate the region of physical parameters that can be reliably measured is presented.
© 2003 Elsevier B.V. All rights reserved.

Many complex fluids, such as foams and emulsions, are multi-phase systems characterized by a very high interfacial area. Often their response to deformation is determined by the properties of the quasi-two-dimensional interfaces, and this makes the study of surface viscoelasticity of great interest [1]. Of course sometimes the two-dimensional dynamics is itself the object of interest. Relatively few experimental techniques exist to probe surface rheology, and surface quasi-elastic light scattering (SQELS) is unique in many respects, such as being a non-invasive and non-perturbative probe. Progress up to 1992 is reviewed in Langevin's monograph [2] and further work is reviewed by Earnshaw in [3]. These sources discuss some of the points summarized in this manuscript in much greater detail and contain references to original work. SQELS has been used to study various *soft matter* systems, including microemulsions, polymer solution interfaces [4,5], bilayer lipid membranes, soap films, surfaces of liquid crystals or gelled systems. In this paper we review one particular use of the SQELS technique, its application to investigating surfaces deco-

rated by monolayers. The dynamics of monolayers of fatty acids, biological lipids, synthetic surfactants and polymers is itself a rich topic, of interest in a wide range of problems that range from understanding biophysical processes to engineering molecular self-assembly. This paper explains how and under what conditions SQELS can be used as a micro-rheological probe of viscoelasticity in a polymer (or polymer-like) monolayer. It will hopefully provide both a clear introduction and an up-to-date reference.

Light scattering from thermal fluctuations of a liquid surface, capillary waves, was first predicted by Smoluchowski in 1908. It was observed experimentally by light-scattering pioneers Mandelstam (1913), Raman (1924) and Gans (1926) but only when laser light sources became available experiments could be attempted to resolve the theoretically predicted [6] frequency spectrum. Katyl and Ingard first observed the spectral broadening of light reflected from methanol and isopropanol surfaces with a Fabry-Perot interferometer [7] and soon after, by using heterodyne spectroscopy, they were able to resolve the Brillouin doublet. They called the surface fluctuations *thermal ripplons* and used an optical setup very similar to that still employed today. The combination of theoretical understanding of surface fluctuation hydrodynamics with the heterodyne optical setup

* Corresponding author.
E-mail address: pc245@cam.ac.uk (P. Cicuta).

provided a precious tool for the study of critical phenomena close to phase transitions in 'simple' fluids. The experiments by Huang and Webb [8] and Meunier [9], determining the critical exponent for the surface tension as a function of temperature close to the critical point, were the first in a long series of studies that used light scattering by surface fluctuations to measure the interface tension. For these investigators this method was important because it enabled non invasive measurements and allowed probing of very low tensions. These two points have remained valid motivations for the use of this technique, as it was further developed and extended to be applied to progressively more complex fluids.

The measurement of the spectral shape of light scattered from a surface covered by a monolayer often enables the determination of intrinsic rheological parameters, in addition to the measurement of surface tension. As this technique relies on observing the dynamics of thermal fluctuations, it is, almost by definition, probing the system's equilibrium state. The frequency of thermal surface roughness fluctuations is typically around 10 kHz and the amplitude is of the order of a few Å, hence although the frequency is high the strain rate is small. As in traditional bulk rheology often one wants to probe the linear response regime. This is not guaranteed by most other surface rheology techniques, from drop dilation to surface shear rheometers [10–13]. These techniques all rely on measuring the system response following a macroscopic external perturbation, which can affect the conformation and structure of a complex system.

Section 1 of this paper describes the theoretical background which is necessary to analyze surface light scattering, that is extracting surface rheological parameters from the spectral shape of scattered light. Understanding the physical processes that give rise to those parameters, for example explaining their dependence on concentration, is a separate problem that will depend on the particular system. This second level of analysis is outside the scope of this paper. The experimental setup is described in Section 2. The methods of SQELS data analysis are presented in Section 3, where an original and practical method is presented to estimate the range of applicability of SQELS. Finally, in Section 4, data on monolayers of the synthetic polymer PVAc is reported as an example of the application of these methods. This system is chosen because it has been studied with SQELS by various authors, and it represents a suitable standard for comparison with the literature.

1. Theory for data analysis on simple monolayers

The theoretical derivation of the spectrum of light scattered by thermal roughness of a surface decorated by a monolayer is due to Lucassen-Reynders and Lucassen [14] and Langevin and Bouchiat [15]. Important considerations have been recently published by Buzza [16] and have resulted in much more robust data analysis. The case

of a decorated surface is an extension of the theoretical description of capillary waves on the clean surface of a fluid. As reviewed in [2], this topic was initially studied by Rayleigh and Mandelstam and was developed further by Levich and Papoular. The problem is to find a solution to the Navier–Stokes equations, which are linearized under the assumption of low velocity which holds for waves with an amplitude small compared to the wave-length:

$$\nabla \cdot \boldsymbol{v} = 0, \tag{1}$$

$$\rho \frac{\partial \boldsymbol{v}}{\partial t} = \nabla \cdot \sigma^{(1,2)}, \tag{2}$$

where the hydrodynamic stress tensor is

$$\sigma^{(1,2)} = \eta_{(1,2)} \left(\frac{\partial v_i}{\partial x_j} + \frac{\partial v_j}{\partial x_i} \right) - P\delta_{ij} \tag{3}$$

and where P and $\boldsymbol{v}$ are the pressure and velocity fields. The flow has to satisfy the boundary conditions of continuous velocity at the interface and of vanishing P and $\boldsymbol{v}$ infinitely far from the interface. If the surface is not flat, P includes the Laplace pressure due to the surface tension.

The same bulk hydrodynamic equations Eqs. (1) and (3) hold in the presence of a monolayer at the interface. The surface film has usually been treated as a mathematically thin plane characterized by a tension, elasticity and viscosity, and it simply contributes additional terms to the stress tensor Eq. (3), as explained clearly in [14]. Thick films or systems with complex interactions with the subphase, like for example diffusion exchange, fall outside of this approximation. Even for this simplest case the process of finding the correct and general constitutive model for interface motion has proven challenging, and remained a long-standing controversial issue. Buzza has shown [16] that many models that have had over time a profound influence in the literature are incorrect. It is proved rigorously that the parametrization by Scriven in terms of a surface tension and complex dilational and shear moduli is the most general possible, and the model is extended to account for relaxation processes in the monolayer. The same paper also clarifies how the models by Goodrich and Kramer [17] erroneously led to consider a complex surface tension, the imaginary part of which was called a transverse viscosity. As a conclusion of ref. [16] a surface wave dispersion relation $D(\omega)$ is found relating the wave frequency to the wavelength. This expression is the same as the original based on Goodrich (see [15]), but with the important difference that the surface tension γ is a real quantity and has to be equal to the equilibrium static surface tension:

$$D(\omega) = [\varepsilon^* q^2 + \mathrm{i}\omega\eta(q+m)] \left[\gamma q^2 + \mathrm{i}\omega\eta(q+m) - \frac{\rho\omega^2}{q} \right] - [\mathrm{i}\omega\eta(m-q)]^2, \tag{4}$$

where m is

$$m = \sqrt{q^2 + \mathrm{i}\frac{\omega\rho}{\eta}}, \quad \mathrm{Re}(m) > 0, \tag{5}$$

η is the subphase Newtonian viscosity, ρ the subphase density, γ the surface tension (or transverse modulus) and ε^* is the complex dilational modulus. Formally, the in-plane modulus measured by SQELS is the sum of the elastic dilation and shear moduli, however the shear modulus is negligible in many polymeric monolayers so the data will be discussed in terms of the dilational modulus only. Solving this equation for $D(\omega) = 0$ gives an expression for the wave frequency, ω, as a function of the wave-vector q. The solutions describe both dilational (in-plane) and transverse waves [14]. In a surface light scattering experiment it is only the transverse waves that scatter light, and power spectrum of scattered light is $P_q(\omega)$ given by [15]:

$$P_q(\omega) = \frac{k_B T}{\pi \omega} \text{Im} \left[\frac{i\omega\eta(m+q) + \varepsilon^* q^2}{D(\omega)} \right]. \tag{6}$$

The behavior of the dilational waves can be inferred from the time evolution of transverse waves because the dynamics of the two modes are coupled through Eq. (4). As will be shown in Section 2, the heterodyne time autocorrelation function which is measured by SQELS is the Fourier transform of the power spectrum given by Eq. (6).

The important practical consequence of Buzza's analysis is that if the surface tension γ is measured independently (and simultaneously to ensure the necessary precision), then only two physical parameters ε and ε' need to be fitted from the experimental data. This is very different from the data analysis of early SQELS experiments, where four fitting parameters where usually considered, and provides a general justification for the correct recent practice (which was motivated by the theory proposed for a specific case [18]) of considering a purely real surface tension. In summary, fitting with a free surface tension parameter should be attempted only if the surface tension cannot be reliably measured independently.

2. Experimental setup

This section describes the experimental aspects of SQELS and the experimental setup used in our laboratory, which is based on the instruments described by Earnshaw [19] and Hård and Neuman [20].

2.1. Optical train

Fig. 1 illustrates the instrument schematically. Two different light sources (L) have been used: a 150 mW single mode diode pumped solid state laser (Laser Quantum, UK) with a wavelength $\Lambda = 532$ nm and a 30 mW He–Ne gas laser (Newport, USA) with a wavelength $\Lambda = 633$ nm. For both lasers, the polarization (horizontal) and intensity are controlled using the combination of a half wave plate and prism polarizer (P). A combination of prism polarizer and neutral density filters can also be used instead. The beam size, profile and collimation are controlled using a spatial filter, S, composed of two microscope objectives and a pinhole. The position of the expansion lens is such that a Gaussian (parallel) beam emerges from the filter assembly, and the choice of focal length determines the beam waist. An appropriate choice of beam diameter has to be made, depending on the physical parameters of the liquid surface under investigation. The optimal condition is detection of scattered light from an area of the surface of the order of the capillary wave coherence length squared. Instrument resolution will become very bad if the illuminated area is much smaller, whereas the signal to noise ratio will fall if the area is too big, in which case one is averaging over uncorrelated dynamics [21].

Photon correlation is done in heterodyne mode (as discussed in detail below), so it is necessary to provide a coherent source of light of the original frequency at the appropriate scattering angle. This is done with a weak diffraction grating (G) which provides a fan of diffracted beams
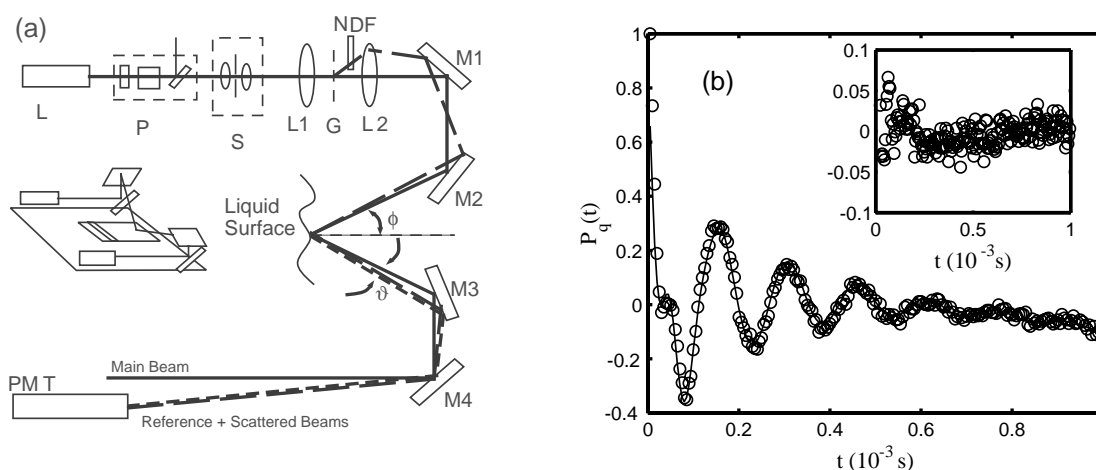

Fig. 1. (a) Diagram of the SQELS optical setup. Each part of the optical train is described in the text. The diagram clearly shows the main beam (solid line), one of the reference beams created by the grating G (dashed line) and the scattered field (dotted line). (b) A correlation function obtained by SQELS at $q = 306$ cm^{-1} on a surface decorated by a PVAc monolayer at surface pressure $\Pi = 3.7$ mN/m, water subphase, $T = 25\,^\circ$C. The solid line is a fit with Eq. (13) as described in the text, and the inset shows the residuals from this fit.

serving as 'reference'. The relative intensity of the reference beams is adjusted by inserting a neutral density filter (NDF) that intercepts the diffracted spots but not the main beam. The lenses L1 ($f = 150$ mm) and L2 ($f = 350$ mm) perform two tasks; they converge the fan of reference beams and the main beam to a single spot at the fluid interface and they focus both the reference beams and the main beam in the front plane of the photomultiplier, situated about 2 m after the surface. In order for the heterodyne signal to dominate the correlation function, the ratio of the intensity of the inelastically scattered light to the 'reference' light must be adjusted to a value of the order of 10^{-3} [22].

The mirrors M1–M2 direct light from the laser onto the liquid surface. A fraction of the light is refracted into the liquid and, to reduce stray light, a mirror on the trough bottom deflects it away from the forward direction. Most of the light is reflected specularly from the surface and a small fraction is scattered by the thermal roughness. The mirrors M3–M4 collect the cone of light in a small solid angle around the main beam, and the mirror M4 is adjusted so that the reference beam (together with the scattered field) is directed into a 1mm diameter aperture in front of the photomultiplier tube. The optical train described above is mounted onto a standard optical table. The liquid surface is contained in a trough resting on an active-damping anti-vibration platform (Mod-2S, Halcyonics, Germany) and situated in a draft-proof enclosure. With the isolation unit active, the laser beam reflected from the liquid surface appears very stable.

2.2. Detected signal

For light polarized in the plane of incidence, the scattering angle θ is related to the capillary wave vector q by:

$$q = \frac{2\pi}{\Lambda} \cos(\phi) \sin(\theta), \qquad (7)$$

where ϕ is the angle of incidence on the liquid surface and Λ is the wave-length of the laser light. The time averaged scattered intensity per solid angle is given by [2]:

$$\frac{dI}{d\Omega} = \frac{I_r(\phi)}{A} \frac{16\pi^2}{\Lambda^4} \cos^3(\phi) \langle |h_q|^2 \rangle_t, \qquad (8)$$

where $I_r(\phi)$ is the reflection coefficient and $\langle |h_q|^2 \rangle_t$ is the mean square amplitude of the mode q surface roughness, which can be easily calculated for an interface in thermal equilibrium [2]:

$$\langle |h_q|^2 \rangle_t = \frac{1}{A} \frac{k_B T}{\gamma q^2}. \qquad (9)$$

Light is detected using a photomultiplier tube (PMT). At the detector the specularly reflected laser beam appears as a central spot, surrounded by a halo of inelastically scattered light (from the liquid surface) and a horizontal series of focused reference spots at 2–3 mm intervals away from the central spot. The total intensity of light falling onto the PMT

is composed of the reference $E_r(t)$ and the scattered $E_s(t)$ light fields [22]:

$$I(t) = I_s(t) + I_r(t) + 2\mathrm{Re}[E_s(t) E_r^*(t)]. \qquad (10)$$

The signal $I(t)$ is processed using a PC-card based photon correlator (BI9000, Brookhaven Instruments, USA). A pulse discriminator is used in the PMT and has been factory-modified to allow the use of the 'multi-photon' mode, originally described by Winch and Earnshaw [23], to increase the sensitivity. The correlator measures the autocorrelation of $I(t)$:

$$\begin{aligned} P(\tau) &= \langle I(t) I(t + \tau) \rangle_t \\ &= (I_s + I_r)^2 + 2 I_s I_r g_s^{(1)}(\tau) + I_s^2 [g_s^{(2)}(\tau) - 1], \qquad (11) \end{aligned}$$

where

$$\begin{aligned} g_s^{(1)}(\tau) &= \frac{\langle E_s(t) E_s(t + \tau) \rangle_t}{\langle I_s(t) \rangle_t} - 1 \quad \text{and} \\ g_s^{(2)}(\tau) &= \frac{\langle I_s(t) I_s(t + \tau) \rangle_t}{\langle I_s^2(t) \rangle_t} - 1 \qquad (12) \end{aligned}$$

are respectively the first and second order normalized autocorrelation functions of the scattered field. $g_s^{(1)}(\tau)$, which is the same as the Fourier transform of the optical spectrum, is the object that needs to be measured [21]. This is possible for $I_r \gg I_s$, when the second term of Eq. (11) dominates the time dependence in the autocorrelation function. Fig. 1(b) shows a typical correlation function with the baseline subtracted and with the amplitude normalized to 1.

2.3. Practical notes

The reference beams are sufficiently weak that the inelastic scattering from them can be ignored, and each reference spot corresponds to light being scattered at a different q value. They were first introduced in this geometry by [24] and serve principally to allow control over the relative intensity of the light fields (thus assuring good heterodyne conditions), to enable repeated experiments at very reproducible scattering angles and to reduce the sensitivity of the setup to surface sloshing which can result in slow oscillations of the reflected reference beams and the scattered field.

In the common use of the instrument, the modulus of the scattering vector, q, and the instrument resolution at a particular reference spot are calibrated at the beginning of each experimental session by fitting the measured correlation function for a pure liquid (typically water) at that scattering angle. During an experiment, and depending on the system studied, various correlation functions are acquired consecutively under the same conditions, with each correlation function accumulated over typically a few minutes. SQELS data can be acquired from monolayers maintained in a Langmuir trough or in other containers such as Petri dishes, provided the diameter is big enough that a central region of the surface is sufficiently flat. For a water–air interface,

below a diameter of 6 cm the de-focusing effect of the curved interface on the reflected beam is very noticeable.

2.4. Instrumental broadening

Soon after the first observation of the broadened power spectrum of light scattered by capillary waves it was recognized that the observed frequency width was inconsistent with the predicted signal for clean liquid surfaces. It took until [25,24] to develop a way of separating out the instrumental broadening due to the optical resolution from the physical signal. The discussion continued in [26–28] on how to take into account the beam propagation through the optical train and on how to optimize the optical design to maximize the resolution. These issues are truly essential only if the instrument is to be used to give absolute values of the (unknown) surface parameters of a certain liquid (of which the bulk parameters have to be known anyway). In the use of the technique to study monolayers, an easier working practice is appropriate: The instrumental parameters (scattering angle and resolution) are calibrated by acquiring the spectrum of scattered light from the clean interface of the subphase, for which both bulk and surface parameters are usually known precisely. Subsequent measurements are performed after spreading the monolayer without any changes taking place on the instrument. The instrumental broadening function has been shown to be adequately approximated by a Gaussian form as discussed in [29]. This allows the resolution to be described by a single parameter, β. In very accurate measurements an improvement could be detected by describing broadening with a two-parameter Voight function [25]. We find the Gaussian broadening correctly accounts for the resolution in our measurements.

2.5. Other hardware configurations

The SQELS setup described above has evolved over many years. Numerous groups have tested and compared different geometries and hardware options, and at the same time purely technological improvements in electronics (the digital correlator and active anti-vibration isolation) and lasers have taken place. It is particularly suited to studying monolayers at the air–liquid surface.

Alternative approaches include a vertical incidence reflection geometry, with a combination of polarized beam-splitter and quarter-wave plate to separate incident and reflected light beams as presented in [28]. A transmission geometry was employed by [30]. This setup is also original in the use of an acousto-optic modulator to provide the reference signal, which enabled access to scattering vectors up to 3×10^4 cm^{-1}, one order of magnitude higher than the maximum attainable with traditional systems [31]. Other setups that make use of a transmission geometry are [32–37]. A transmission geometry has the advantages of requiring a simpler optical train and reduces the sensitivity of the technique to slow oscillations (*sloshing*) of the surface. Other approaches

to minimizing sloshing are discussed by [38]. The main limit of the transmission geometry is that only systems with a negligible scattering from the liquid subphase can be studied.

The specific issue of cost in building a surface scattering setup was addressed in [32], where the possibility of using a cheap light source (multi-mode diode laser) and intensity detection (silicon photodiode) is explored. A further simplification is to use optical fibers instead of the optical train, as in the setup described in [34]. This has the additional advantage of enabling a more compact and robust instrument. Thanks to progress in computer power, in the near future it should become possible to substitute the digital correlator with a (relatively inexpensive) dedicated data acquisition board, feeding data to a personal computer and performing real time software based correlations [39]. As a testament to the maturity of the technique, it is significant to reference an educational paper [40] where SQELS is suggested as an appropriate experiment in an undergraduate student course.

Various research groups are actively studying polymer monolayers with SQELS. We review this research over the past ten years, after the publication of Langevin's monograph [2]. The group of Richards has done extensive work on polymer monolayers, some of which is covered in the monograph [41]. Recent measurements on multiblock copolymers are reported in [42]. The group of Monroy, Ortega and Rubio has worked on monolayers of polymers and polymer mixtures. In their work monolayer parameters are extracted from the fitted values of frequency and damping obtained from the power spectrum, an approach which is critically discussed in Section 3. SQELS has been used to study the viscoelasticity of model polymer monolayers such as PVAc [43,44], PVAc and P4HS blends [45], and P4HS [46]. In addition to capillary wave data, this group has, for some systems, presented comparative measurements obtained by different techniques [43,46], providing valuable data spanning a very wide frequency range. The group of Yu also studied model polymers representative of good and θ solvent conditions [47]. Diblock copolymers are studied in [48]. In a recent paper [49] light scattering results on monolayers of six different polymers are reviewed and compared.

2.6. Technical details

Fig. 2 shows the range of scattering vectors q that can be measured with the SQELS apparatus. The values of the corresponding capillary wave frequency (Fig. 2(a)) and damping constant (Fig. 2(b)) are shown in log plots. The slopes, as expected in this range [22], are in agreement with the first order approximations that can be made to Eq. (4), as is well documented in the literature [2]. The instrumental resolution values that are measured for different scattering angles are shown in Fig. 2(c), where it is clear that the instrument setup employing the 533 nm laser had a considerably better resolution than the 633 nm laser. The setups also had slight differences in positioning the optical train, so that different beam waists were obtained.
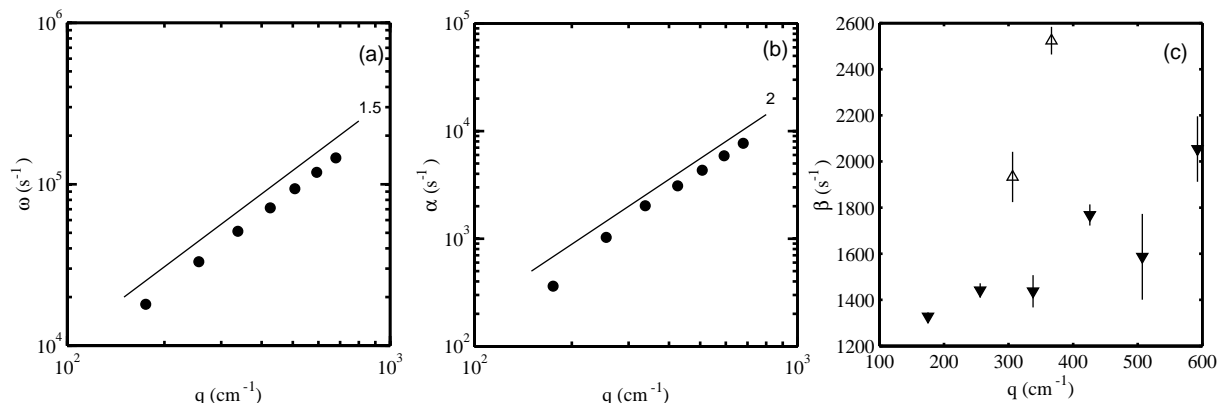
Fig. 2. Log–Log plots of (a) the frequency and (b) the damping factor of capillary waves as a function of the wave-vector, obtained by fitting data with Eq. (15). Data is obtained on a clean water surface at 22 °C. The solid lines are approximated solutions to Eq. (4), known as the Kelvin and Stokes laws [2]. (c) Instrumental resolution (parameter β in Eq. (13)) as a function of the scattering wave-vector. ($\triangle$) data acquired with the 532 nm laser beam, and ($\blacktriangle$) data are typical of the setup with the 633 nm laser. The resolution depends strongly on the laser beam waist.

It is well known that a range of time-delay channels on the digital correlator should be selected so that the full extent of the decay of the correlation function is measured. However it can happen in SQELS experiments that for some scattering angles it is difficult to find an optimum match of channel times to correlation decay. With our setup, this happens for the smallest scattering angles. It was found that if the channels were chosen as to cut-off the correlation function, this had a *very* strong effect when fitting the data with our software program, described below. This is because the discrete Fourier transform routine assumes periodic boundary conditions on the data (other routines pad the data with zeros, which would also lead to the same problem). Hence, if the data has not decayed to a flat baseline, there is the possibility that the correlation function, which is approximately a damped cosine oscillation, does not match the periodicity of its symmetric image at large times. This problem has a characteristic signature: a bad fit and large residues are found at the largest correlator times. When such flawed data is fitted, it leads to either negative values of the resolution parameter or to negative values of ε'. In numerous papers in the literature it is clear that the time correlation data has been cut off, and this problem is not acknowledged. Usually, the cut-off does not hide important features of the correlation function, and the data can be used. However whilst fitting, it is essential to ensure that the correlation function connects with its symmetric image without loss of periodicity, for example by careful choice of the number of channels that are analyzed.

3. Data analysis

3.1. Direct spectral analysis

The maximum information that can be extracted on the surface parameters of a monolayer from the time correlation (or the frequency power spectrum) of light scattered from capillary waves is obtained by fitting the data directly, with the theoretical model given in Eqs. (4) and (6). As discussed in Section 2, our setup measures the time correlation function, which is related to Eq. (6) by [29]:

$$P_q(t) = B + A\,\text{F.T.}\,[P_q(\omega)]\exp\left(-\frac{\beta^2 t^2}{4}\right) + \text{droop} \\ + \text{fast after-pulse}, \tag{13}$$

with A and B instrumental parameters and where the 'droop' and 'after-pulse' terms are added to correct for slow surface oscillations and fast phototube after-pulse respectively. They have the forms:

$$\text{droop} = -\mathrm{d}t^2, \quad \text{fast after-pulse} = f_1\cos[f_2 t]\exp[-t/f_3] \tag{14}$$

.

We follow Earnshaw's approach to data analysis [29]. Our fitting program is coded in Fortran. In essence, a non-linear curve fitting of the model Eq. (13) to the SQELS time correlation data is carried out in the time domain, where analytical approximations to account for instrumental parameters such as broadening, 'droop' due to surface sloshing and the amplitude of a fast phototube 'after-pulse' are known (Eq. (14)). However, the theoretical model Eq. (6) gives the power spectrum of light in the frequency domain, so at every fitting step the Fourier transform of the model data is performed, and then the instrumental corrections are applied. Rather than describing in greater detail the fitting program, which is very similar to Earnshaw's, it is worth presenting our fitting methodology, and how it has improved since the original presentation.

The most important point is that it is now clear that some of the parameters introduced in [29] can be measured independently and should thus not be subject to fitting when analyzing an unknown monolayer. In particular the resolution parameter β in Eq. (13) (which measures the instrumental broadening discussed in Section 2.4) is strongly correlated to the parameters determining the spectral shape, despite
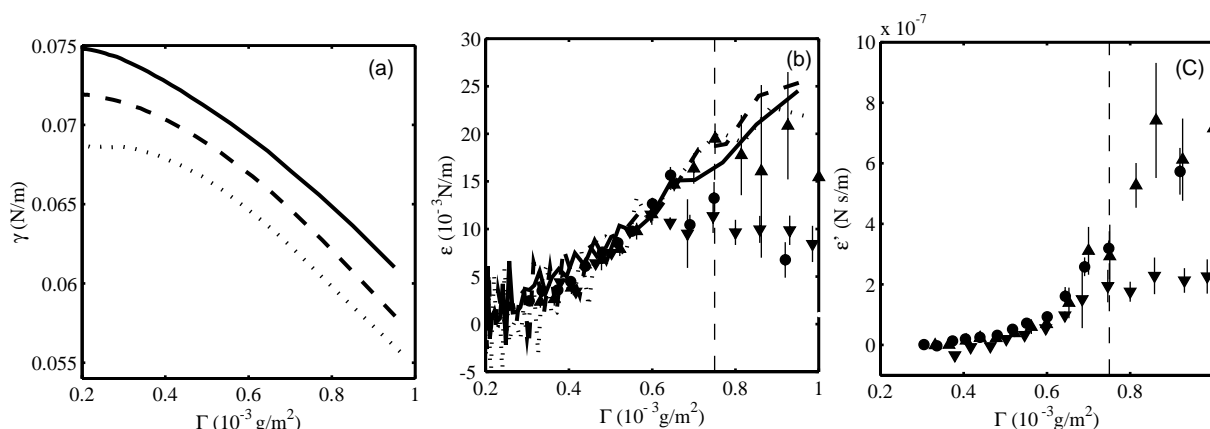
Fig. 3. Surface parameters of PVAc monolayers. (a) Surface tension, measured with a Wilhelmy plate. Solid, dashed and dotted lines correspond respectively to 6, 25 and 45 °C. (b) Dilational elastic modulus and (c) dilational viscosity, obtained by fitting SQELS data with Eq. (13). Symbols correspond to the subphase temperature: (▲) $T = 6$ °C, (●) $T = 25$ °C and (▼) $T = 45$ °C. The lines in (b) are the equilibrium dilational moduli obtained from isotherm experiments. As discussed in the text, the surface tension is fixed to the static value during SQELS data analysis. Initial fit parameters are $\varepsilon = 10^{-3}$ N/m and $\varepsilon' = 10^{-8}$ Ns/m. In the low concentration region, no systematic effect was noted by fitting with other reasonable initial values. In the high concentration region, values of ε less than equilibrium, which is un-physical [16], resulted even with very high initial values. The vertical dashed lines delimit the regions where the fitted values become un-physical, see the text and Fig. 5.

having a different functional form. This leads to very unstable fitting unless β is separately determined as a fixed instrumental parameter. It can be estimated by analyzing data from a clean water surface, together with the best value for the scattering vector q.

Given Buzza's conclusion that the surface tension is to be fixed to the static value (and if the tension is accessible to measurements by other means), then only the following parameters are free to be determined from the fit of an experimental correlation function with Eq. (13):

- Two "physical parameters": ε and ε'.
- Four "signal corrections": The amplitude A, background B, droop coefficient d and amplitude of fast phototube after-pulse f_1. The parameters f_2 and f_3 are determined separately by fitting the phototube signal of light directly from the laser.

We measure the surface tension with the Wilhelmy plate method, simultaneously to the acquisition of the light scattering signal. Values of ε and ε' obtained by fitting data directly are shown in Fig. 3(b) and (c). We will discuss the range over which such fits are valid in Section 3.3.

3.2. Phenomenological fitting

An alternative approach to data analysis is to fit the time correlation function with a damped cosine function:

$$P_q(t) = B + A \cos (\omega t + \phi) \exp (-\alpha t) \exp \left(-\frac{\beta^2 t^2}{4} \right),$$
(15)

plus the droop and after-pulse terms of Eq. (14). This expression, having three parameters in addition to the four signal

corrections described above, provides an excellent approximation of the correlation function calculated using the dispersion relation [41,16]. As with the data analysis described in Section 3.1, the final term in Eq. (15) is the instrumental broadening, which should be calibrated separately. ω and α are the frequency and damping constant of the capillary wave oscillations, and ϕ is a phase term that accounts for the deviation of the power spectrum from a Lorentzian form. No knowledge of the nature of the interface is required for this analysis, and the fitting procedure is very stable. This is in fact the only meaningful analysis of the ripplon spectrum that is possible if one does not have a model that provides a dispersion equation to relate the ripplon spectrum to the microscopic surface moduli [18], a situation that occurs for example for a heterogeneous monolayer [50]. In the literature, it is often found that data is fitted with Eq. (15), and then either the fitted frequency and damping are quoted (seldom are values of the phase ϕ reported), or a search for interfacial properties which would be consistent with these values is attempted. Ref. [49] provides a very good explanation of this method. However this approach is not ideal. Firstly, all three parameters (ω, α, ϕ) should in general be reported, as they are needed to correctly interpolate the data. Secondly if, using the results of this fit, the search for values of the surface parameters that are consistent through Eq. (4) with the fitted (ω, α, ϕ) is attempted, then this is an unnecessary approximation to testing Eq. (4) directly on the data with the direct spectral analysis fit described in Section 3.1.

In conclusion, the most reliable surface parameters should result from fitting the data directly, with Eq. (13), when this fit is stable. In the next section it will be shown that the fit will work well only in a limited region of physical parameters. Outside of this region, the fitted values of Eq. (15) become the only data that can be discussed. Although a good fit

with Eq. (15) is always obtained, one should not be misled: this approach too will yield information on ε and ε' only in the same limited range that will be estimated below. Indeed for large ε and ε' the phenomenological fitted values saturate to a constant limit [49] which only depends on the surface tension. The only advantage of the phenomenological fitting approach is that the fit remains stable over the whole concentration range, whereas the fit with the physical parameters (Eq. (13)) becomes unstable (and can yield un-physical values of the dilational parameters) as the boundary of the region of strong coupling between in-plane and out-of-plane modes is approached.

3.3. Estimating the valid fitting region

It is generally acknowledged in the SQELS literature on monolayers that data analysis fitting the power spectrum with Eqs. (4) and (6) (or the correlation function with Eq. (13)) becomes more difficult as the parameters ε and ε' become large [2,49,52]. This is because the power spectrum of scattered light tends to become independent of the dilational moduli in the limit of large ε or ε' where the in-plane and out-of-plane modes will have a very different characteristic frequency. It is important to establish where is the boundary of the surface parameter region that can be explored. Here a method is presented to estimate the range of ε and ε' where the SQELS time correlation data can be expected to be reliably fitted.

The method of estimating the reliable region of surface parameters is based on using the stable and reliable fit with the phenomenological Eq. (15) to give an estimate of the experimental error that is intrinsic to surface light scattering data. It can be summarized in the following steps:

(1) Generating model data with Eqs. (4), (6) and (13), with fixed γ and over a wide range of physical parameters: $-100 < \varepsilon(\text{mN/m}) < 100$ and $-5 < \varepsilon'(10^{-7}\text{Ns/m}) < 20$;
(2) Fitting the modeled data with Eq. (15), thus establishing three maps: $(\varepsilon, \varepsilon') \rightarrow \omega$; $(\varepsilon, \varepsilon') \rightarrow \alpha$; $(\varepsilon, \varepsilon') \rightarrow \phi$;
(3) Finding, for each fitted value $(\omega_{\text{fit}}, \alpha_{\text{fit}}, \phi_{\text{fit}})$, the values of $(\varepsilon, \varepsilon')$ that map into a region $(\omega_{\text{fit}} \pm \delta\omega, \alpha_{\text{fit}} \pm \delta\alpha, \phi_{\text{fit}} \pm \delta\phi)$, where these error bands are estimates of the experimental error intrinsic to the SQELS signal, obtained by measuring the spread in the results of fits with Eq. (15) on 10 separate sets of real data;
(4) Recording the spread in each of the ε and ε' sets that map into $(\omega_{\text{fit}} \pm \delta\omega, \alpha_{\text{fit}} \pm \delta\alpha, \phi_{\text{fit}} \pm \delta\phi)$;
(5) Determining the region in the parameter space $(\varepsilon, \varepsilon')$ that generates data which will be distinguishable to SQELS.

The results of such an investigation are presented in Fig. 5. For a realistic range of $(\varepsilon, \varepsilon')$, Fig. 5 shows the spread in the fitted values that can be expected when fitting SQELS data. In practice such figures serve to identify the range of surface parameters where the technique works well. In all of

Table 1
ω_0 and α_0 are the values of the phenomenological frequency and damping parameters fitted on a clean water surface with Eq. (15), for two different experiments that represent the range of conditions encountered

Parameter	Average conditions	Best conditions
q (cm^{-1})	306	507
ω_0 (s^{-1})	42000	94000
α_0 (s^{-1})	1300	4500
$\delta\omega$ (s^{-1})	225	140
$\delta\alpha$ (s^{-1})	254	145
$\delta\Phi$	0.12	0.023

$\delta\omega$, $\delta\alpha$ and $\delta\Phi$ are the spread of the fitted values over 10 independent correlation function measurements at identical conditions, and they are the best indicator of the intrinsic experimental error. The values $\delta\omega$, $\delta\alpha$ and $\delta\Phi$ are used, as described in the text, to estimate the valid fitting regions which are drawn in Fig. 5.

the panels, the surface tension $\gamma = 65\,\text{mN/m}$ and subphase conditions correspond to water at $T = 20\,^\circ\text{C}$. Very similar results (not shown) are obtained for $\gamma = 75$ and $55\,\text{mN/m}$. As explained above, to generate Fig. 5 the measured error in the experimental data is used, and this depends on various experimental conditions which determine the signal to noise ratio. The data used to generate the two conditions represented in Fig. 5 is summarized in Table 1. The largest experimental error bands correspond to the poorest quality data that can still be usefully analyzed, such as shown in Fig. 1(b). The 'best' quality error bands correspond to the data shown in ref. [51]. In general it is clear that the region of good coupling between the transverse an in-plane modes is quite sharply delimited. In particular, it can be seen that reliable fits for the dilational modulus ε can be expected in the worst conditions only for $\varepsilon < 25\,\text{mN/m}$ and $\varepsilon' < 4 \times 10^{-7}\,\text{Ns/m}$. In the best conditions the region is larger and extends to $\varepsilon < 55\,\text{mN/m}$ and $\varepsilon' < 5 \times 10^{-7}\,\text{Ns/m}$. Reliable fits for the dilational viscosity ε' can be expected in the worst conditions for a quite limited region $\varepsilon < 20\,\text{mN/m}$ and $\varepsilon' < 3 \times 10^{-7}\,\text{Ns/m}$, but in the best conditions the area increases considerably to $\varepsilon < 55\,\text{mN/m}$ and $\varepsilon' < 10 \times 10^{-7}\,\text{Ns/m}$ with a reasonable confidence in the results.

4. A model polymeric monolayer

Poly(vinyl acetate) (PVAc) is well known as a polymer that forms surface monolayers which are well described by 'good-solvent' conditions within the two-dimensional semi-dilute statistical model for polymers [53]. As commented by Jones and Richards [41], PVAc monolayers have been measured with SQELS by various groups, following initial work by Langevin [54]. This makes it an ideal monolayer to study for comparing experimental and data analysis methods with the literature. We do not consider studies where data was fitted attempting to find an imaginary component for the surface tension, an approach which is now recognized as incorrect [16]. The studies that we consider for comparison are from Yu's group [52,47,49]
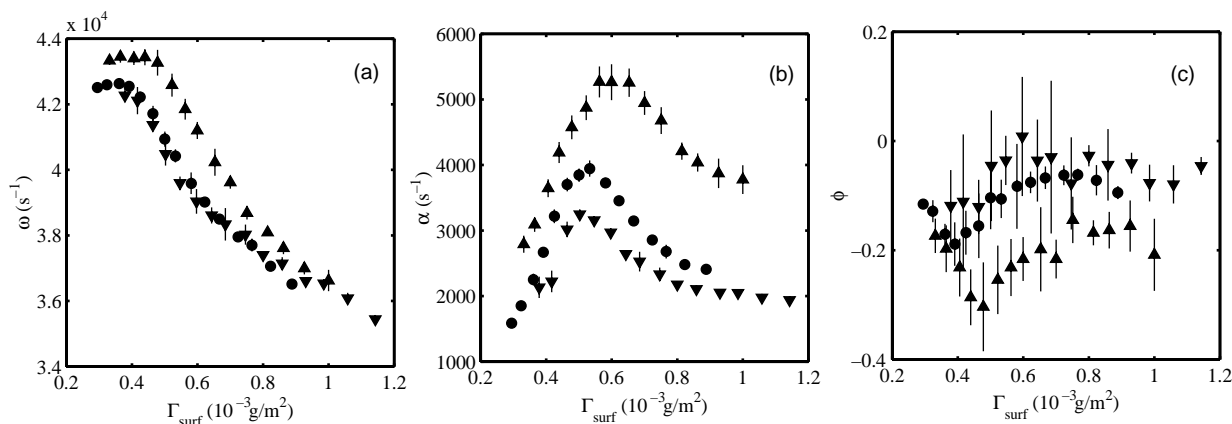
Fig. 4. Phenomenological parameters of PVAc monolayers at different temperatures, determined by fitting SQELS correlation functions with Eq. (15): (a) frequency, (b) damping coefficient, (c) phase term. The symbols correspond to the same conditions described in Fig. 3.

and Monroy's group [43,45,44]. In the experiments of Yu et al. data was obtained over a narrow range of wavevectors $323 < q\,(\mathrm{cm}^{-1}) < 445$, while Monroy et al. acquired data for $115 < q\,(\mathrm{cm}^{-1}) < 804$. Both groups studied the effect of concentration and temperature on the dilational modulus and viscosity. While there is a qualitative agreement of all experiments finding that the SQELS and equilibrium dilational moduli are the same in the semi-dilute regime, the data of dilational viscosity differs rather widely. Further-

more, Monroy et al. find a strong dependence on temperature [44], while Yu et al. had found no such effect [47]. Both groups perform data analysis following the 'phenomenological fitting' approach discussed above. There seems to be inconclusive data from the different experiments particularly at high concentration. We are not concerned here with the possible experimental details leading to such different behavior in similar systems. Instead, we present new data on PVAc that is analyzed by 'direct fitting' as discussed in
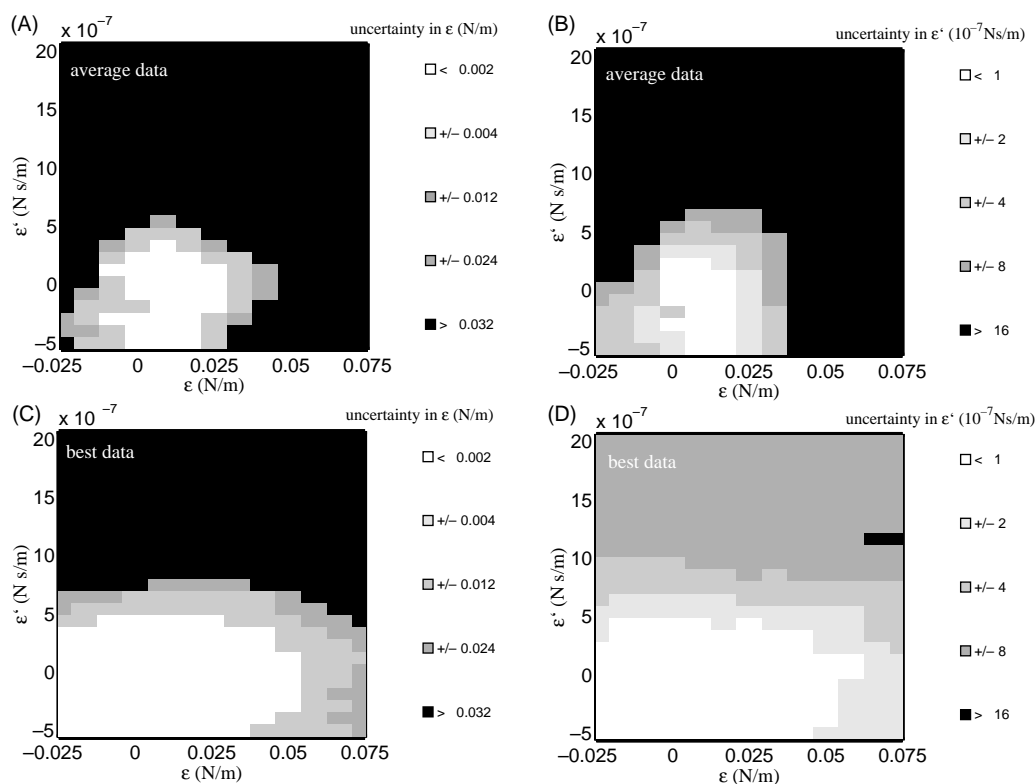

Fig. 5. Figures showing in white the region in the $(\varepsilon, \varepsilon')$ plane where the SQELS data is expected to give reliable fits for ε (left panels) and for ε' (right panels). As marked on the figures, the top panels have been calculated under average experimental conditions, at $q = 306\,\mathrm{cm}^{-1}$ and poor signal to noise ratio, corresponding to the data shown in Fig. 1(b). The bottom panels are under the best conditions achieved with the instrument described here, and correspond to the data shown and discussed in ref. [51] at $q = 507\,\mathrm{cm}^{-1}$. The legends indicate quantitatively the extent of the $(\varepsilon, \varepsilon')$ region that will give experimentally indistinguishable correlation functions. The data from which these results are calculated is summarized in Table 1.

the previous sections, and we extend the comments on the valid region for fitting to discuss the literature data.

4.1. SQELS on PVAc monolayers

Experiments are performed under conditions very similar to ref. [43]. Solutions of PVAc (Acros 183255000, $M_w = 170,000$, used as received) 0.12 mg/ml in tetrahydrofurane, are spread on a pure water subphase, at different temperatures. The monolayer forms spontaneously and is compressed in a Langmuir trough. SQELS data is acquired at a given set of concentrations. The concentration range which is explored is within the semi-dilute regime, that is for concentrations below the maximum in the equilibrium dilational modulus [51].

Fig. 4 shows the parameters obtained by a 'phenomenological fit'. They are typical of polymer monolayers described by the dispersion relation Eq. (4). In particular, the decrease of the frequency ω with concentration is due to the reduction of surface tension, and the peak in the damping coefficient α has been shown to occur at the resonance condition between in-plane and out-of-plane modes [41]. Traditionally, it is from these fitted parameters that the values of dilational modulus and viscosity are extracted by further analysis. As described above, we follow the alternative 'direct fitting' method. It is extremely important to accurately measure the subphase temperature and use the corresponding values of density and viscosity. Fig. 3(b) and (c) show the dependence of ε and ε' on the concentration. Also shown on the figures is the limit beyond which the time correlation data does not depend on ε and ε', as calculated in Fig. 5 for 'average data' conditions. It is clear that the discrepancy above the concentration $\Gamma_{surf} \simeq 0.6 \times 10^{-3}$ g/m^2 between the equilibrium dilational modulus and ε obtained from SQELS is most likely due to the parameters being outside the fitting region. A similar situation occurs for the protein films studied in [51], at higher values of the moduli because the raw data quality was better, see Fig. 5 under 'best data' conditions. It is now clear that the large scattering in results on PVAc reported by Monroy et al. and Yu et al. at high concentration is probably due to the surface moduli being outside the reliable fitting region.

In the low concentration region, where the PVAc data presented here can be fitted reliably, we find that ε is equal to the equilibrium value and that there is not any significant effect of temperature. We can compare the values of ε' to those in the literature and find good agreement with ref. [43], while ref. [52] reports values that are lower by almost an order of magnitude.

5. Conclusions

Surface light scattering is a non-invasive and sensitive technique that can be used to study the dilational rheology of polymer monolayers on a liquid subphase. The experimental setup and theoretical framework have been described, and the method of data analysis has been discussed in depth. It has been shown that reliable fits can be obtained for a limited range of surface parameters. In particular it has been emphasized that for large values of dilational modulus, such as will be attained by typical polymer monolayers at a high monomer concentration or by fatty acid layers in the condensed phases, it becomes impossible to determine the magnitude of the modulus from the light scattering data. Experimental data on PVAc monolayers has been presented here to give an example of the methods discussed in the paper and to bring attention to the uncontrolled approximations that lie behind the widely used 'phenomenological fitting' approach.

References

[1] D.M.A. Buzza, C.-Y.D. Lu, M.E. Cates, Linear shear rheology of incompressible foams, J. Phys. II France 5 (1995) 37.

[2] D. Langevin, Light Scattering by Liquid Surfaces and Complementary Techniques, Dekker, New York, 1992.

[3] J.C. Earnshaw, Light scattering as a probe of liquid surfaces and interfaces, Adv. Colloid Interface Sci. 68 (1996) 1.

[4] Q.R. Huang, C.H. Wang, Effects of viscoelasticity of bulk polymer solution on the surface modes as probed by laser light scattering, J. Chem. Phys. 109 (1998) 6103.

[5] H. Nakanishi, S. Kubota, Absence of surface mode in a visco-elastic material with surface tension, Phys. Rev. E 58 (1998) 7678.

[6] V.G. Levich, Physicochemical Hydrodynamics, Prentice-Hall, Englewood Cliffs, 1962.

[7] R.H. Katyl, U. Ingard, Line broadening of light scattered from a liquid surface, Phys. Rev. Lett. 19 (1967) 64.

[8] J.S. Huang, W.W. Webb, Viscous damping of thermal excitations on the interface of critical fluid mixtures, Phys. Rev. Lett. 23 (1969) 160.

[9] J. Meunier, Diffusion de la lumière par les ondes de surface sur CO$_2$ près du point critique mesure de la tension superficielle, J. Phys. France 30 (1969) 933.

[10] R. Miller, R. Wüstneck, J. Krägel, G. Kretzschmar, Kilational and shear rheology of adsorption layers at liquid interfaces, Colloids Surf. A 111 (1996) 75.

[11] C. Barentin, C. Ybert, J.-M. di Meglio, J.-F. Joanny, Surface shear viscosity of Gibbs and Langmuir monolayers, J. Fluid Mech. 397 (1999) 331.

[12] C.F. Brooks, G.G. Fuller, C.W. Curtis, C.R. Robertson, An interfacial stress rheometer to study rheological transitions in monolayers at the air-water interface, Langmuir 15 (1999) 2450.

[13] J. Ding, H.E. Warriner, J.A. Zasadzinski, D.K. Schwartz, Magnetic needle viscometer for Langmuir monolayers, Langmuir 18 (2002) 2800.

[14] E.H. Lucassen-Reynders, J. Lucassen, Properties of capillary waves, Adv. Colloid Interface Sci. 2 (1969) 347.

[15] D. Langevin, M.A. Bouchiat, Spectrum of thermal fluctuations of a liquid covered by a thin film, Comptes Rendus Acad. Sci. 272B (1971) 1422.

[16] D.M.A. Buzza, General theory for capillary waves and surface light scattering, Langmuir 18 (2002) 8418.

[17] L. Kramer, Theory of light scattering from fluctuations of membranes and monolayers, J. Chem. Phys. 55 (1971) 2097.

[18] D.M.A. Buzza, J.L. Jones, T.C.B. McLeish, R.W. Richards, Theory of surface light scattering from a fluid-fluid inetrface with adsorbed polymeric surfactants, J. Chem. Phys. 109 (1998) 5008.

[19] J.C. Earnshaw, R.C. McGivern, Photon correlation spectroscopy of thermal fluctuations of liquid surfaces, J. Phys. D: Appl. Phys. 20 (1987) 82.

[20] S. Hård, R.D. Neuman, Laser light-scattering measurements of viscoelastic mono-molecular films, J. Colloid Interface Sci. 83 (1981) 315.

[21] B.J. Berne, R. Pecora, Dynamic Light Scattering, Wiley, New York, 1976.

[22] J.C. Earnshaw, Surface light scattering: a methodological review, Appl. Optics 36 (1997) 7583.

[23] P.J. Winch, J.C. Earnshaw, A method for rapid data acquisition in photon-counting experiments for time-dependent systems, J. Phys. E—Sci. Instrum. 21 (1988) 287.

[24] S. Hård, Y. Yamnerius, O. Nilsson, Laser heterodyne apparatus for measurements of liquid surface properties-Theory and experiments, J. Appl. Phys. 47 (1976) 2433.

[25] D. Langevin, Light scattering from the free surface of water, J. Chem. Soc. Faraday Trans. I 70 (1974) 95.

[26] L.B. Shih, Surface fluctuation spectroscopy: a novel technique for characterizing liquid interfaces, Rev. Sci. Instrum. 55 (1984) 716.

[27] J.A. Mann, R.V. Edwards, Surface fluctuation spectroscopy: comments on experimental techniques and capillary ripplon theory, Rev. Sci. Instruments 55 (1984) 727.

[28] R.B. Dorshow, A. Hajiloo, R.L. Swofford, A surface laser-light scattering spectrometer with adjustable resolution, J. Appl. Phys. 63 (1988) 1265.

[29] J.C. Earnshaw, R.C. McGivern, A.C. McLaughlin, P.J. Winch, Light-scattering studies of surface viscoelasticity: direct data analysis, Langmuir 6 (1990) 649.

[30] K. Sakai, P.-K. Choi, H. Tanaka, K. Takagi, A new light scattering technique for a wide-band ripplon spectroscopy at the MHz region, Rev. Sci. Instrum. 62 (1991) 1192.

[31] C.J. Hughes, J.C. Earnshaw, High frequency capillary waves: a light scattering spectrometer, Rev. Sci. Instrum. 64 (1993) 2789.

[32] T.M. Jorgensen, A low-cost surface laser light scattering spectrometer, Meas. Sci. Technol. 3 (1992) 588.

[33] Z. Zhang, I. Tsuyumoto, S. Takahashi, T. Kitamori, T. Sawada, Monitoring of molecular collective behavior at a liquid/liquid interface by a time-resolved quasi-elastic laser scattering method, J. Phys. Chem. A 101 (1997) 4163.

[34] P. Tin, J.A. Mann, W.V. Meyer, T.W. Taylor, Fiber-optics surface-light-scattering spectrometer, Appl. Optics 36 (1997) 7601.

[35] W.V. Meyer, J.A. Lock, H.M. Cheung, T.W. Taylor, P. Tin, J.A. Mann, Hybrid reflection-transmission surface light-scattering instrument with reduced sensitivity to surface sloshing, Appl. Optics 36 (1997) 7605.

[36] A. Trojánek, P. Krtil, Z. Samec, Quasi-elastic laser light scattering from thermally excited capillary waves on polarised liquid—liquid interfaces, Part 1: effects of adsorption of hexadecyltrimethylammonium chloride at the water—1,2-dichloroethane interface, J. Electroanal. Chem. 517 (2001) 77.

[37] J.A. Mann Jr., P.D. Crouser, W.V. Meyer, Surface fluctuation spectroscopy by surface-light-scattering spectroscopy, Appl. Optics 40 (2001) 4092.

[38] W.V. Meyer, G.H. Wegdam, D. Fenistein, J.A. Mann Jr., Advances in surface-light-scattering instrumentation and analysis: noninvasive measuring of surface tension, viscosity, and other interfacial parameters, Appl. Optics 40 (2001) 4113.

[39] D. Magatti, F. Ferri, Fast multi-tau real-time software correlator for dynamic light scattering, Appl. Optics 40 (2001) 4011.

[40] D.G. Miles Jr., Z. Yang, H. Yu, Surface light scattering adapted to the advanced undergraduate laboratory, J. Chem. Educ. 79 (2002) 1007.

[41] R.A.L. Jones, R.W. Richards, Polymers at Surfaces and Interfaces, Cambridge University Press, Cambridge, UK, 1999.

[42] A.J. Milling, R.W. Richards, R.C. Hiorns, R.G. Jones, Surface viscoelatic properties of spread films of a polysilylene-poly(ethylene oxide) multiblock copolymer at the air/water interface, Macromolecules 33 (2000) 2651.

[43] F. Monroy, F. Ortega, R.G. Rubio, Dilational rheology of insoluble polymer monolayers: poly(vinylacetate), Phys. Rev. E 58 (1998) 7629.

[44] F. Monroy, F. Ortega, R.G. Rubio, Thermoelastic behavior of polyvinylacetate monolayers at the air-water interface: evidences for liquid-solid phase transition, Eur. Phys. J. B 13 (2000) 745.

[45] F. Monroy, F. Ortega, R.G. Rubio, Rheology of a miscible polymer blend at the air-water interface: quasielastic surface light scattering study and analysis in terms of static and dynamic laws, J. Phys. Chem. B 103 (1999) 2061.

[46] F. Monroy, S. Rivillon, F. Ortega, R.G. Rubio, Dilational Rheology of Langmuir polymer monolayers: poor-solvent conditions, J. Chem. Phys. 115 (2001) 830.

[47] K.-H. Yoo, H. Yu, Temperature dependence of polymer film properties on the air-water interface: Poly(vinyl acetate) and poly(n-butyl methacrylate), Macromolecules 22 (1989) 4019.

[48] F.E. Runge, M.S. Kent, H. Yu, Capillary wave investigation of surface films of diblock copolymers on an organic subphase: poly(dimethylsiloxane)-poly(styrene) films at the air/ethyl benzoate interface, Langmuir 10 (1994) 1962.

[49] A.R. Esker, L. Zhang, B.B. Sauer, W. Lee, H. Yu, Dilational viscoelastic behaviors of homopolymer monolayers: surface light scattering analysis, Colloids Surf. A 171 (2000) 131.

[50] P. Cicuta, I. Hopkinson, Dynamic light scattering from colloidal fractal monolayers, Phys. Rev. E 65 (2002) 041404.

[51] P. Cicuta, I. Hopkinson, Studies of a weak polyampholyte at the air-buffer interface: the effect of varying pH and ionic strength, J. Chem. Phys. 114 (2001) 8659.

[52] M. Kawaguchi, B.S. Sauer, H. Yu, Polymeric monolayer dynamics at the air/water interface by surface light scattering, Macromolecules 22 (1989) 1735.

[53] R. Vilanove, F. Rondelez, Scaling description of two-dimensional chain conformations in polymer monolayers, Phys. Rev. Lett 45 (1980) 1502.

[54] D. Langevin, Light-scattering study of monolayer viscoelasticity, J. Colloid Interface Sci. 80 (1981) 412.